Vortex plume distribution in confined turbulent rotating convection

2013 EPL 104 54002

(http://iopscience.iop.org/0295-5075/104/5/54002)

A Letters Journal Exploring the Frontiers of Physics

December 2013

EPL, **104** (2013) 54002
doi: 10.1209/0295-5075/104/54002

www.epljournal.org

Vortex plume distribution in confined turbulent rotating convection

Rudie P. J. Kunnen[1(a)], Yoann Corre[1(b)] and Herman J. H. Clercx[1,2]

[1] *Fluid Dynamics Laboratory, Department of Applied Physics and J. M. Burgers Center for Fluid Dynamics, Eindhoven University of Technology - P.O. Box 513, 5600 MB Eindhoven, The Netherlands, EU*
[2] *Department of Applied Mathematics and J.M. Burgers Center for Fluid Dynamics, University of Twente P.O. Box 217, 7500 AE Enschede, The Netherlands, EU*

received 17 September 2013; accepted in final form 6 December 2013
published online 2 January 2014

PACS 47.55.pb – Thermal convection
PACS 47.32.Ef – Rotating and swirling flows

Abstract – Vortical columns are key features of rapidly rotating turbulent Rayleigh-Bénard convection. In this work we probe the structure of the sidewall boundary layers experimentally and show how they affect the spatial vortex distribution in a cylindrical cell. The cell has a diameter-to-height aspect ratio 1/2 and is operated at Rayleigh number 5.9×10^9 and Prandtl number 6.4. The vortices are detected using particle image velocimetry. We find that for inverse Rossby numbers $1/Ro \gtrsim 3$ (expressing the rotation rate in a dimensionless form) the sidewall boundary layer exhibits a rotation-dependent thickness and a characteristic radial profile in the root-mean-square azimuthal velocity with two peaks rather than a single peak typical for the non-rotating case. These properties point to Stewartson-type boundary layers, which can actually cover most of the domain for rotation rates just above the transition point. A zonal ordering of vortices into two azimuthal bands at moderate rotation rates $3 \lesssim 1/Ro \lesssim 7$ can be attributed to the sidewall boundary layer. Additionally, we present experimental confirmation of the tendency of like-signed vortices to cluster on opposite sides of the cylinder for $1 \lesssim 1/Ro \lesssim 5$. At higher rotation rates and away from the sidewall the vortices are nearly uniformly distributed.

Introduction. – Rotating Rayleigh-Bénard convection (RRBC) is a simple model system for the investigation of flows in which buoyancy and rotation play an important role. Examples include oceanic convection [1], the interior of gaseous planets [2] and the core dynamics of the Earth responsible for its magnetic field [3]. RRBC is experimentally most conveniently studied in a rotating upright cylinder, where the fluid inside is heated from below and cooled from above. We refer to ref. [4] for a recent review of RRBC. For such a geometry there are four governing parameters. The Rayleigh number $Ra = g\alpha\Delta T H^3/(\nu\kappa)$ quantifies the destabilizing temperature gradient. Here g is the gravitational acceleration, α is the thermal expansion coefficient of the fluid, ΔT is the applied temperature difference, H is the height of the fluid layer, and ν and κ are the kinematic viscosity and thermal diffusivity of the fluid, respectively. The Prandtl number $\sigma = \nu/\kappa$ describes the diffusive properties of the fluid, the inverse Rossby number $1/Ro = \tau_c/\tau_\Omega$ expresses the ratio of the convective time scale $\tau_c = \sqrt{H/(g\alpha\Delta T)}$ to the rotational time scale $\tau_\Omega = 1/(2\Omega)$, with Ω the angular velocity. Finally, the aspect ratio $\Gamma = D/H$, with cylinder diameter D, describes the geometry.

There have been many recent investigations of turbulent RRBC [5–21]. In geometries for which $\Gamma \approx 1$ the rotational dependence of heat transfer and flow structuring are quite well known [4]. For $\Gamma = 1$ there is a sharp transition at $1/Ro_c \approx 0.4$ from a large-scale circulation (LSC), a domain-filling convection roll, at $1/Ro < 1/Ro_c$ to a flow consisting of an array of columnar vortices for $1/Ro > 1/Ro_c$. This transition is accompanied by a remarkable heat-transfer increase for fluids with $\sigma > 1$ [4]. The LSC is known to perform an anticyclonic (counter-rotating) precession [5]. LSC dynamics are commonly studied with sidewall temperature probes, where cosine-shaped azimuthal profiles are fitted to detect the LSC [15,21].

(a) E-mail: r.p.j.kunnen@tue.nl
(b) Visiting student from Université Paris-Sud - 91405 Orsay cedex, France, EU.

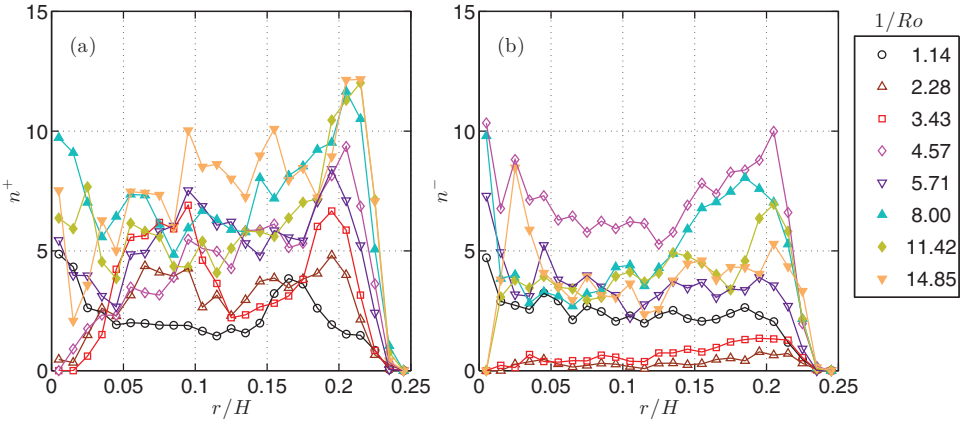

Fig. 1: (Colour on-line) Time-averaged vortex densities as a function of radial position r at several rotation rates $1/Ro$. (a) Density n^+ of cyclonic vortices. (b) Density n^- of anticyclonic vortices.

However, in a recent study [21] of a $\Gamma = 1/2$ cell many results were found which were very much unlike the findings for $\Gamma = 1$. The transition from LSC to columnar vortices is dependent on geometry: for $\Gamma = 1/2$ it is expected at $1/Ro_c \approx 0.86$ based on heat-transfer measurements and modelling [20,21]. For $1/Ro > 1/Ro_c$ these authors found a strong, persistent LSC signature from sidewall temperature measurements. Additionally, the LSC appeared to precess *cyclonically* (corotating).

These observations raise questions on the flow structuring. Which flow arrangement leads to the persistent LSC-like temperature signature and how can it display the counterintuitive cyclonic drift? Partial answers have been found with recent numerical simulations [22]. The persistent LSC-like azimuthal temperature profiles have been reproduced, but it has been noted that instead of an LSC there was an array of vortical columns as the dominant flow structure. The authors noted that the separate clustering of cold downgoing and hot upgoing vortices also leads to a cosine-shaped temperature profile.

We have investigated RRBC in a $\Gamma = 1/2$ cylinder under rapid rotation with *in situ* planar velocimetry to further address these open questions. We find new effects due to the presence of the sidewall: clustering and zonal ordering of vortices. The Stewartson-type sidewall boundary layers —which we recently studied in detail [18,23]— are clearly influencing the vortex distribution.

The experiment. – In this letter we present results of particle image velocimetry (PIV) measurements in our new cylindrical convection cell with aspect ratio $\Gamma = 1/2$ which is otherwise of similar design to our previous $\Gamma = 1$ cell [13]. It is made of Plexiglas, has a height $H = 400\,\mathrm{mm}$ and a diameter $D = 200\,\mathrm{mm}$. It is filled with water that is seeded with nearly neutrally buoyant polyamid particles of size $50\,\mu\mathrm{m}$. The cylinder is closed from below with a copper block that is electrically heated. At the top a sapphire window separates the cylinder volume from a transparent cooling chamber; cooling water is circulated through this chamber. The mean temperature is kept at $T_m = 24\,^\circ\mathrm{C}$ while top and bottom temperatures differ by $\Delta T = 5\,^\circ\mathrm{C}$. The Rayleigh number is $Ra = 5.9 \times 10^9$ and the Prandtl number is $\sigma = 6.4$. The cell is placed on a rotating table. Several rotation rates $0.09 \leq \Omega \leq 1.3\,\mathrm{rad/s}$ have been applied, so that $1.0 \leq 1/Ro \leq 14.8$.

A laser light sheet crosses the cell horizontally at a height $z = 0.9H$ close to the top plate but well outside the boundary layer of thickness δ/H between 0.002 and 0.008 depending on the rotation rate. A charge coupled device camera with spatial resolution 1600×1200 pixels and 12-bits dynamic range records the motions of the tracer particles in the laser light sheet. The smaller side of the camera view covers almost the full diagonal extent of the cell, so that a nearly full cross-section can be measured. The camera images are post-processed with a PIV algorithm; the resulting velocity field consists of vectors of the in-plane horizontal velocity components on a regular grid with spatial separation $\Delta x = \Delta y = 2.6\,\mathrm{mm}$. Images are recorded at 15 Hz. Recordings lasted between 20 and 30 minutes. All of the velocity data presented in this letter are normalised by the convective velocity scale $U = H/\tau_c = \sqrt{g\alpha\Delta T H} = 0.070\,\mathrm{m/s}$.

Vortex detection. – At rotation rates $1/Ro > 1/Ro_c \approx 0.86$ an unsteady array of columnar vortices is expected. Indeed, visualizations of velocity fields from the current measurements at $1/Ro > 1$ reveal that coherent vortices are the dominant flow structures. To find the vortices we resort to the Q_{2D} criterion as applied before by us in ref. [24], which compares the rate-of-strain and the rotational parts of the 2D velocity gradient tensor to discern vortices (negative Q_{2D}) from strain-dominated regions in the flow (positive Q_{2D}). The threshold for vortex detection is set to $-Q_{2D,\mathrm{rms}}$. Contours of Q_{2D} at the threshold level can then be analysed to find the vortex area and its centroid, which we shall use as the location of the vortex. The sign of vorticity at the centroid is used to discern cyclonic vortices with positive vertical vorticity $\omega_z > 0$ and

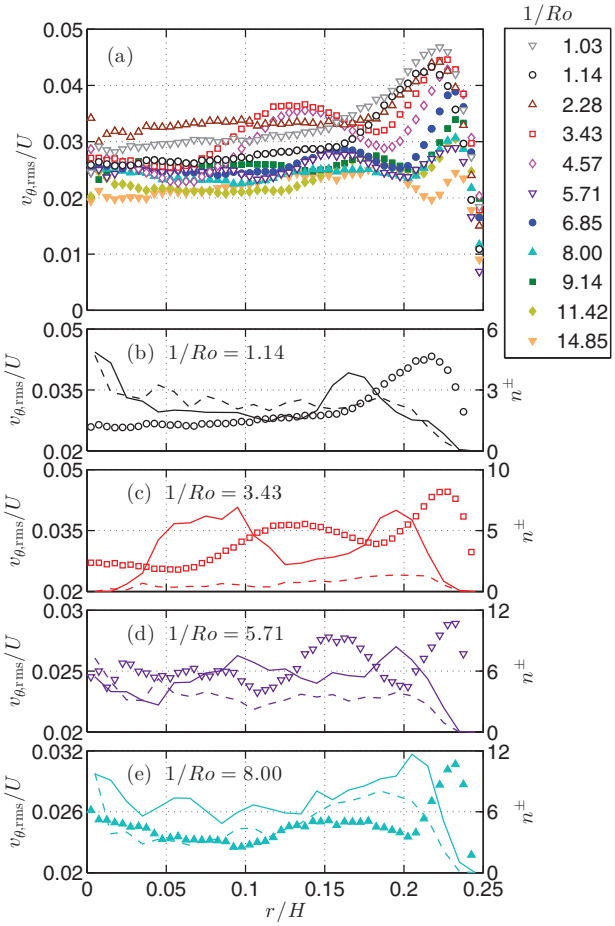

Fig. 2: (Colour on-line) (a) Radial profiles of root-mean-square azimuthal velocity $v_{\theta,\mathrm{rms}}$, normalised with the convective velocity U. (b)–(e): comparison of radial $v_{\theta,\mathrm{rms}}$ profiles (symbols, left ordinate) and radial vortex density profiles (lines, right ordinate) n^+ (solid lines) and n^- (dashed lines), at four rotation rates: $1/Ro = 1.14$ (b), $1/Ro = 3.43$ (c), $1/Ro = 5.71$ (d), $1/Ro = 8.00$ (e).

anticyclonic vortices with $\omega_z < 0$. Using this method we have counted the number of (anti)cyclonic vortices $N^{\pm}(r)$ in radial shells of width $\Delta r = 4\,\mathrm{mm}$ as a function of radius r, using snapshots separated by 1/3 s. They are converted into areal vortex number densities as a function of radius r as $n^{\pm}(r) = N^{\pm}(r)A/A_{\mathrm{shell}}(r)$, where A is the full cross-sectional area and $A_{\mathrm{shell}}(r)$ the corresponding shell area. The value of n^+ (n^-) indicates how many cyclonic (anticyclonic) vortices would be found within the cylinder cross-section in case it was uniformly filled with cyclonic (anticyclonic) vortices at the given density.

Zonal ordering and sidewall boundary layer. – Vortex densities $n^{\pm}$ are plotted in fig. 1. For clarity we do not include all considered rotation rates. There are several remarkable observations. i) In all cases a rather large number of vortices is detected. We do not observe two dominant vortices at this height, in qualitative correspondence with the visualisations from numerical simulation results by Stevens *et al.* [22] given the current measurement height. ii) For all rotation rates, the vortex density is highest at a position relatively close to the sidewall ($r = H/4$). This has been noted before in numerical simulations [25] although for lower Ra. iii) For $3 \lesssim 1/Ro \lesssim 7$ there are "zonal bands" where the vortex density is higher, most prominently for $1/Ro = 3.43$ (open red squares). iv) Especially at $1/Ro = 4.57$ the cyclonic vortex density is low in the centre while the anticyclonic distribution is more uniform, which is the topic of the next section.

The distributions of vortices can be compared with radial profiles of the root-mean-square (rms) azimuthal velocity $v_{\theta,\mathrm{rms}}$, plotted in fig. 2(a). The rms velocity typically reveals a maximal value close to the sidewall; the position of the peak is often used to represent the thickness of the boundary layer (BL). For the lowest values of $1/Ro \leq 2.28$ included in the figure there is indeed a single maximum. However, starting from $1/Ro = 3.43$ there are two maxima that both shift towards the sidewall as $1/Ro$ is increased. There is a prominent change in the BL structure around $1/Ro \approx 3$. This change is also reflected in the vortex distribution, as is visualised in fig. 2(b)–(d): $v_{\theta,\mathrm{rms}}$ is low at the radial positions where vortex number density is high, and vice versa. This vortex density effect is prominent for cyclonic vortices, but absent for their anticyclonic counterparts. At the highest rotation rates ($1/Ro = 8.00$ and higher) the sidewall bands are thinner and the vortex density peak interior to the innermost maximum of $v_{\theta,\mathrm{rms}}$ is no longer observed (fig. 2(e)).

To gain more insight into the zonal band structure we have calculated the thickness δ_ν of the sidewall BL from the radial positions of the maxima of $v_{\theta,\mathrm{rms}}$. These thicknesses are plotted as a function of $1/Ro$ in fig. 3 with open red symbols. The positions of the second maximum ($\delta_{\nu,\mathrm{2nd}}$) and the minimum in between (δ_{min}) are also included whenever they occur. It is found that at $1/Ro \lesssim 3$ the sidewall BL thickness is hardly affected by rotation, as was also true for $\Gamma = 1$ [13]. For $1/Ro \gtrsim 3$, however, it exhibits the signature of a Stewartson layer with a thickness that goes as $\delta_\nu/H = E^{1/3}$, where $E = \nu/(\Omega H^2)$ is the Ekman number. Note that there is no prefactor in this relation. We have considered Stewartson layers in rotating cylindrical convection before [18,23]. The BL structure is rather convoluted: a mean circulation consisting of a downdraft at the sidewall and an updraft adjacent to it is found in the upper half of the domain $z > 0.5H$, with a mirrored circulation for $z < 0.5H$. The flow in the underlying $E^{1/4}$ layer [23] is a higher-order contribution in the small parameter E and therefore cannot be distinguished here. This circulation is persistent in the turbulent flow; its structure can nevertheless quite accurately be described with solutions of the stationary, linearised equations of motion. From the current analysis it is apparent that the vortices are expelled from the regions of high $v_{\theta,\mathrm{rms}}$, which are related to the BL circulation. At appropriate rotation rates the vortices gather with higher density inside the

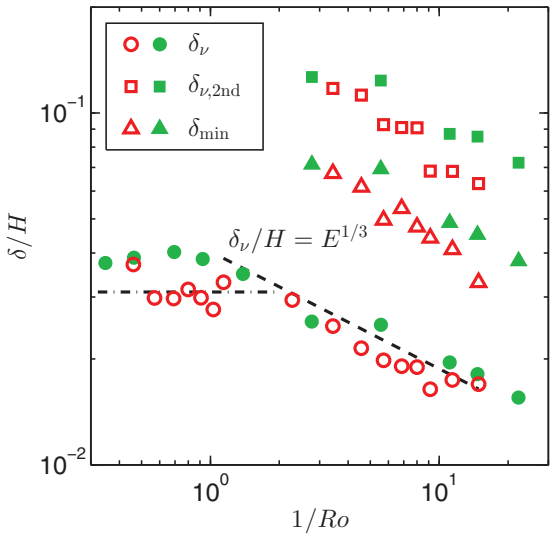

Fig. 3: (Colour on-line) Dependence on $1/Ro$ of the sidewall BL thickness δ_ν (circles). The positions of the second maximum ($\delta_{\nu,2\mathrm{nd}}$, squares) and the minimum ($\delta_{\min}$, triangles) of $v_{\theta,\mathrm{rms}}$ are also included. The open red symbols are the current experimental results at $\Gamma = 1/2$ and $Ra = 5.9 \times 10^9$. The dashed line represents the corresponding theoretical Stewartson BL thickness $\delta_\nu/H = E^{1/3}$ [18,23]. The dash-dotted line is included as a guide to the eye. Filled green symbols represent reexamined numerical data from ref. [13] at $\Gamma = 1$, $Ra = 1.0 \times 10^9$, evaluated also at $z = 0.9H$.

BL circulation and just adjacent to it, leading to the two peaks in the vortex density. For $1/Ro \geq 8.00$, however, the boundary-layer circulation apparently is too weak to form a barrier for the vortices; a single vortex density peak close to the sidewall remains [25]. This edge effect bears resemblance to wall effects as encountered in 2D molecular-dynamics simulations using disks, where the disks are geometrically forced into an ordered layer state with higher number density near a wall.

Concerning the positions of the second maximum and the minimum of $v_{\theta,\mathrm{rms}}$, it is found that they exhibit approximately the same scaling with rotation as δ_ν. A remarkable observation is that at $1/Ro = 3.43$ the sidewall BL apparently covers most of the cross-sectional area. In fig. 2(c) and fig. 3 it is found that the second maximum of $v_{\theta,\mathrm{rms}}$ is found at $r/R \approx 0.5$ ($R = H/4$ is the cylinder radius), implying that approximately 75% of the total cylinder cross-section is taken up by the sidewall boundary layer. It is probable that this BL coverage can be extended even further by exploring the transitional $1/Ro$ range in more detail. We expect that the transition to Stewartson BLs is actually triggered by the geometry (analogous to the transition between LSC and vortical plumes [10,16,20]) rather than a transition in the balance of Coriolis and buoyancy forces as expressed by $1/Ro$.

We have also reexamined the numerical data of our previous investigation on a $\Gamma = 1$ convection cell [13], now at a height $z = 0.9H$. Similar double-peaked $v_{\theta,\mathrm{rms}}$ profiles are found for $1/Ro > 2$, but not displayed here. The positions of the two maxima and the minimum in between are included in fig. 3 with filled green symbols. The BL scales reveal a similar dependence on $1/Ro$. In general the BL thickness at this lower $Ra = 1.0 \times 10^9$ is slightly larger than in the current experiment at higher $Ra = 5.9 \times 10^9$. The value of $1/Ro$ at which the transition to a Stewartson-type BL takes place cannot be determined with certainty from the simulation results at $\Gamma = 1$; it must be within the range $1 < 1/Ro < 2$.

We thus find strong indications that the zonal ordering of vortices near the sidewall is caused by the Stewartson BLs. The zonal ordering of vortices is observed for rotation rates at which Stewartson BLs are formed, *i.e.* $1/Ro \gtrsim 3$, and they apparently affect the distributions of vortices throughout the domain by setting up mean flow patterns [23]. At large enough $1/Ro \geq 8$ the height of the innermost $v_{\theta,\mathrm{rms}}$ peak is reduced; the correlation with the reduced vortex density has vanished. A more uniform vortex distribution is found. However, at all of the considered values of $1/Ro$ there is a distinct peak of vortex density close to the sidewall [25].

Vortex clustering. – It has been postulated [21] and demonstrated [22] that the persistence of the cosine-shaped azimuthal temperature profiles in the range where no LSC is expected can be explained by vortex clustering: like-signed vortices clustering on azimuthally opposite sides of the domain also represent such a thermal signature, indistinguishable from an LSC. We investigate clustering of like-signed vortices by calculating the centroid $\boldsymbol{x}_c^+$ ($\boldsymbol{x}_c^-$) of the ensemble of cyclonic (anticyclonic) vortices for a given snapshot as the averaged positions $\boldsymbol{x}_i^+$ ($\boldsymbol{x}_i^-$) of the detected cyclonic (anticyclonic) vortices. Of course, these vortex centroids move in time. We calculate the distance $r_c^\pm = |\boldsymbol{x}_c^\pm|$ from the centroids to the centre for all the considered snapshots, removing the azimuthal dependence for increased statistics. The variation of $r_c^\pm$ over the radial coordinate r is expressed in the PDFs $P[r_c^\pm](r)$. For example, $P[r_c^+](r)\mathrm{d}r$ denotes the probability of finding the centroid of the cyclonic vortices in a thin shell of radius r and thickness $\mathrm{d}r$ around the centre. The PDFs are normalised such that $\int_0^{H/4} P[r_c^\pm](r)\mathrm{d}r = 1$. Some of these PDFs $P[r_c^+](r)$ and $P[r_c^-](r)$ are depicted in figs. 4(a) and (b), respectively. Several curves at other $1/Ro$ values are omitted for clarity of the figures.

The shapes of the PDF curves vary a lot with $1/Ro$. For $1/Ro \geq 8.00$ the distributions have the same shape. We show only one for clarity of the figure. For an azimuthally uniform vortex distribution the centroid should always be at $r = 0$. In order to construct a reference PDF, we individually calculate the mean and standard deviation (SD) of the x and y coordinates of $\boldsymbol{x}_c^\pm$. Here it is found for $1/Ro = 8.00$ that the SDs of the x and y coordinates of $\boldsymbol{x}_c^+$ are roughly the same and equal to 16 mm, while the means of both coordinates are zero. The composite distribution of $r_c^+ = |\boldsymbol{x}_c^+|$ with this SD as the

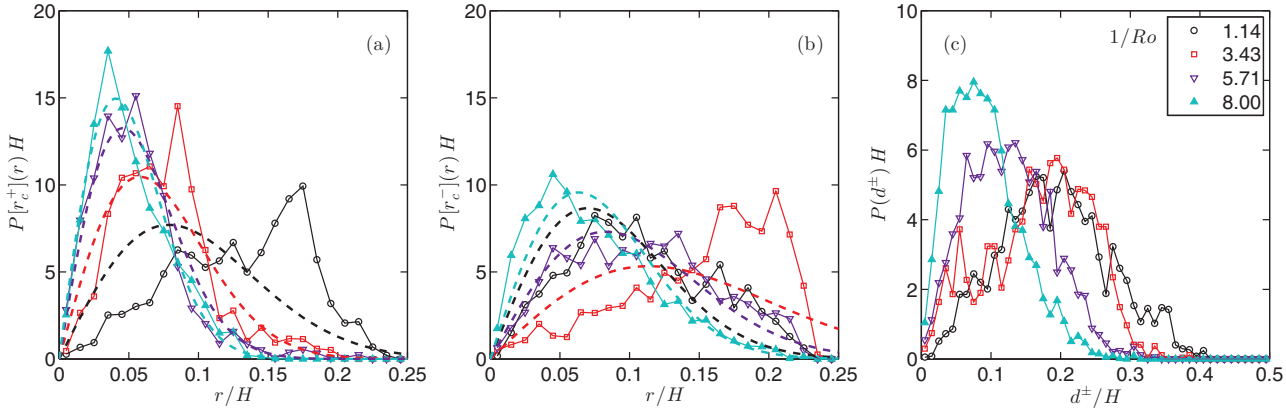

Fig. 4: (Colour on-line) (a) PDFs of the distance r_c^+ of the positive-vortex centroid $\boldsymbol{x}_c^+$ to the centre (solid lines with symbols). The dashed lines are reference PDFs based on a Gaussian distribution in both x and y with zero mean and standard deviation equal to the measurement. (b) PDFs $P[r_c^-](r)$ for the negative vortices (solid lines with symbols). The dashed lines are reference PDFs based on a Gaussian distribution in both x and y with zero mean and standard deviation equal to the measurement. (c) PDF of the distance $d^\pm$ between the positive-vortex centroid $\boldsymbol{x}_c^+$ and the negative-vortex centroid $\boldsymbol{x}_c^-$.

combination of Gaussian distributions in x and y with zero mean and that SD is shown in fig. 4(a) with a dashed line in the same colour as the corresponding PDF. The composite distribution matches well with the measured PDF at $1/Ro = 8.00$. For all other PDFs a similar procedure is followed to define reference PDFs; they are included in fig. 4(a), (b) as dashed lines with the same colours as the original PDFs. The PDFs at $1/Ro = 5.71$ (purple down-triangles) also match rather well with their corresponding reference curves. This hints at a nearly uniform vortex distribution with the centroid preferentially found near the centre, but due to the larger SD the centroid can wander further from the centre than at $1/Ro = 8.00$. Additionally, the PDF of r_c^- reveals a slightly higher probability in the tail at larger r values, indicating a slight off-centre preference for this centroid.

For $1 \lesssim 1/Ro \lesssim 5$ the PDFs are broad and may even peak at high r values, indicating that an off-centre centroid position may be likely with correspondingly a non-axisymmetric vortex distribution. This is also inferred from the reference PDFs. At lower values of $1/Ro$ below 8.00 the shape of the PDFs indicate that they are not composed of Gaussian distributions, so a uniform distribution is not evident in those cases. We thus conclude that the centroids are located preferentially at off-centre positions for moderate rotation rates $1 \lesssim 1/Ro \lesssim 5$.

Now that it is found that like-signed vortices can gather around centroids at off-centre locations, the positions of the centroids relative to each other must be investigated to verify whether the two are spatially separated. It is straightforward to calculate for all considered times the distance between the centroids as $d^\pm = |\boldsymbol{x}_c^+ - \boldsymbol{x}_c^-|$. Of course, $d_\pm$ fluctuates in time as well. The PDF of $d^\pm$ is shown in fig. 4(c). It is found that for $1 \lesssim 1/Ro \lesssim 5$ the clusters can be separated by rather large distances, comparable to and even surpassing the radius $R = H/4$ of the cylinder. In those cases the two centroids are located on opposite sides in the cross-section. Such an arrangement would lead to a cosine-like azimuthal profile of temperature near the sidewall [21] at this measurement height $z = 0.9H$: the vortices originating at the top plate (which are cyclonic at this height) carry cold fluid downwards on one side of the cell, while on the opposite side vortices coming from the bottom plate (which are anticyclonic at this height) carry hot fluid upwards. The PDFs for $1/Ro > 8.00$ are again left out for clarity; they are very similar to the $1/Ro = 8.00$ curve.

The clustering of like-signed vortices can be related to vortex-vortex interactions: like-signed vortices tend to attract each other which can even lead to merger [26]. Why, then, is the clustering halted for $1/Ro \geq 8.00$? The transition appears to coincide with the observed transition in the zonal ordering of vortices, shown earlier in this letter. It may be that the vortex trapping by the sidewall BL plays a role here as well. Alternatively, it is known that in rapidly rotating convection the vortical tubes are shielded, *i.e.* that they develop a ring of oppositely signed vorticity around their cores [27–29]. The shields reduce the mutual interactions of vortices. At higher values of $1/Ro$, stronger shields may prevent vortex interactions. Unfortunately, we cannot prove the formation of shields from the current measurements. Given that we required a total cross-sectional view, the spatial resolution is too coarse. A more detailed investigation of the shields is warranted.

It has been mentioned before that the vortex clustering can explain the LSC-like temperature profiles as measured by Weiss and Ahlers [21]. They found that the LSC-like profile precessed in cyclonic direction for $1/Ro \leq 1.75$ at $Ra = 4.5 \times 10^9$, which most resembles the Ra value applied here. It is a natural next step to investigate the azimuthal motion of the centroids to try and explain

the observed precession. It is found (but not shown here) that they precess anticyclonically in the entire range $1 < 1/Ro \lesssim 5$ for which vortex clustering is observed. Unfortunately, the noisy data are ill suited for quantitative evaluation other than the sign of precession. For $1/Ro > 1.75$ the current results and those reported in [21] are consistent in a qualitative sense. For $1 < 1/Ro \leq 1.75$ the inconsistent dynamics could reflect the different experimental conditions: in the current work a transparent, less insulating sidewall is required to allow for illumination. To resolve the discrepancy it is advised to consider both flow velocity and temperature near the sidewalls. A DNS approach as in [22] could be used to clarify the relation between temperature and velocity in the near-wall regions.

Conclusion. – We report on the effects of the sidewall on the vortex distribution in strongly turbulent rotating convection. At all rotation rates there is a maximum of vortex density close to the sidewall, which resembles the near-wall layering effect found in 2D molecular dynamics. The Stewartson layers that are formed on the sidewall for $1/Ro \gtrsim 3$ may cover large portions of the flow domain at appropriate rotation rates. They exhibit a two-peak radial structure in the root-mean-square azimuthal velocity profiles, leading to a zonal ordering of vortices with a higher vortex density between the two peaks. Additionally, like-signed vortices tend to cluster for $1 \lesssim 1/Ro \lesssim 5$: cyclonic and anticyclonic vortices form clusters on opposite sides of the cylinder. The occurrence of clusters and their dynamics can at least partially explain the sidewall temperature measurements of Weiss and Ahlers [21]. At the highest rotation rates the Stewartson layers are thin and their influence on the vortex distribution is minor. The vortices may develop shields that reduce their interaction. Nearly uniform vortex distributions are found for $1/Ro \geq 8$.

This letter presents a new regime division of rapidly rotating RBC, after our previous suggestions based on velocity statistics [13] or heat transfer [18]. The numbers are similar but they show some quantitative differences. We expect that several processes contribute to these changes in behaviour, that different transition values can be found depending on which statistics are used. Additionally, it is certainly dependent on Ra, σ and Γ.

The sidewalls affect cylindrical RRBC in more ways than we anticipated before. The distinction between bulk and boundary layer is not as clear as in non-rotating convection, especially not for rotation rates near the transition to Stewartson BLs. For experimental investigations that should reflect convective flow without sidewalls, in other words to reach a flow with a bulk range that is unaffected by sidewall effects, we recommend to use a container of large enough aspect ratio. For conventional containers with $\Gamma \leq 1$, the sidewalls become irrelevant only at rather large rotation rates.

REFERENCES

[1] Marshall J. and Schott F., *Rev. Geophys.*, **37** (1999) 1.
[2] Busse F. H., *Chaos*, **4** (1994) 123.
[3] Roberts P. and Glatzmaier G., *Rev. Mod. Phys.*, **72** (2000) 1081.
[4] Stevens R. J. A. M., Clercx H. J. H. and Lohse D., *Eur. J. Mech. - B/Fluids*, **40** (2013) 41.
[5] Hart J. E., Kittelman S. and Ohlsen D. R., *Phys. Fluids*, **14** (2002) 955.
[6] Vorobieff P. and Ecke R. E., *J. Fluid Mech.*, **458** (2002) 191.
[7] Kunnen R. P. J., Clercx H. J. H. and Geurts B. J., *Phys. Rev. Lett.*, **101** (2008) 174501.
[8] Kunnen R. P. J., Clercx H. J. H. and Geurts B. J., *EPL*, **84** (2008) 24001.
[9] Zhong J.-Q., Stevens R. J. A. M., Clercx H. J. H., Verzicco R., Lohse D. and Ahlers G., *Phys. Rev. Lett.*, **102** (2009) 044502.
[10] Stevens R. J. A. M., Zhong J.-Q., Clercx H. J. H., Ahlers G. and Lohse D., *Phys. Rev. Lett.*, **103** (2009) 024503.
[11] Liu Y. and Ecke R. E., *Phys. Rev. E*, **80** (2009) 036314.
[12] King E. M., Stellmach S., Noir J., Hansen U. and Aurnou J. M., *Nature (London)*, **457** (2009) 301.
[13] Kunnen R. P. J., Geurts B. J. and Clercx H. J. H., *J. Fluid Mech.*, **642** (2010) 445.
[14] Niemela J. J., Babuin S. and Sreenivasan K. R., *J. Fluid Mech.*, **649** (2010) 509.
[15] Zhong J.-Q. and Ahlers G., *J. Fluid Mech.*, **665** (2010) 300.
[16] Weiss S., Stevens R. J. A. M., Zhong J.-Q., Clercx H. J. H., Lohse D. and Ahlers G., *Phys. Rev. Lett.*, **105** (2010) 224501.
[17] Stevens R. J. A. M., Clercx H. J. H. and Lohse D., *New J. Phys.*, **12** (2010) 075005.
[18] Kunnen R. P. J., Stevens R. J. A. M., Overkamp J., Sun C., van Heijst G. J. F. and Clercx H. J. H., *J. Fluid Mech.*, **688** (2011) 422.
[19] Liu Y. and Ecke R. E., *Phys. Rev. E*, **84** (2011) 016311.
[20] Weiss S. and Ahlers G., *J. Fluid Mech.*, **684** (2011) 407.
[21] Weiss S. and Ahlers G., *J. Fluid Mech.*, **688** (2011) 461.
[22] Stevens R. J. A. M., Clercx H. J. H. and Lohse D., *Phys. Rev. E*, **86** (2012) 056311.
[23] Kunnen R. P. J., Clercx H. J. H. and van Heijst G. J. F., *J. Fluid Mech.*, **727** (2013) 509.
[24] Kunnen R. P. J., Clercx H. J. H. and Geurts B. J., *Phys. Rev. E*, **82** (2010) 036306.
[25] Stevens R. J. A. M., Overkamp J., Lohse D. and Clercx H. J. H., *Phys. Rev. E*, **84** (2011) 056313.
[26] Cerretelli C. and Williamson C. H. K., *J. Fluid Mech.*, **475** (2003) 41.
[27] Sprague M., Julien K., Knobloch E. and Werne J., *J. Fluid Mech.*, **551** (2006) 141.
[28] Portegies J. W., Kunnen R. P. J., van Heijst G. J. F. and Molenaar J., *Phys. Fluids*, **20** (2008) 066602.
[29] Grooms I., Julien K., Weiss J. B. and Knobloch E., *Phys. Rev. Lett.*, **104** (2010) 224501.